

Reactive Hot Pressing of ZrB₂–SiC–ZrC Composites at 1600°C

Wen-Wen Wu,^{‡,§} Guo-Jun Zhang,^{*,†,‡} Yan-Mei Kan,[‡] and Pei-Ling Wang[‡]

[‡]State Key Laboratory of High Performance Ceramics and Superfine Microstructures, Shanghai Institute of Ceramics, Shanghai 200050, China

[§]Graduate School of the Chinese Academy of Sciences, Beijing 100000, China

A ZrB₂–SiC–ZrC ceramic was produced by reactive hot pressing using Zr, Si, and B₄C as raw materials. The kinetics of the reaction process was studied. The reduction of powders by ball milling is of crucial importance for the sintering. The self-propagating high-temperature synthesis reaction between the raw powders can be ignited by controlling the sintering conditions, which leads to a sintering temperature as low as 1600°C, the lowest sintering temperature reported thus far. The relative density is 97.3%, with an open porosity of 0.6%, and the mechanical properties are comparable to the composites that sintered at higher temperatures. The depletion of oxygen impurities during the sintering was discussed.

I. Introduction

IN the last few years, efforts in developing hypersonic aerospace vehicles and reusable atmospheric reentry vehicles led to a significant increase in the interest in ultra-high-temperature ceramics (UHTCs).^{1–3} For their use as thermal protection systems of sharp leading edges of these vehicles, UHTCs need to have a high melting point (> 3000°C) along with good oxidation resistance at temperatures above 1800°C.⁴ Zirconium and hafnium-based ceramics (borides, carbides, and nitrides) possess a number of unique properties, including extremely high melting temperatures and hardnesses, low volatilities, and good thermal and electrical conductivities. Of these, ZrB₂ also has the lowest theoretical density (6.09 g/cm³), as well as good thermal shock resistance and the ability to form dense outer layers of B₂O₃ that could decrease the oxidation of the material at temperatures below 1100°C.^{5,6} Often, SiC is added to ZrB₂ to enhance its oxidation resistance and improve the bend strength by limiting grain growth during densification.^{7,8}

Considering the poor sinterability of the strongly covalent compounds,⁹ ZrB₂ is usually densified by pressure-assisted sintering techniques at temperatures > 1900°C. Researchers have carried out much work to improve the sintering behavior of the ZrB₂-based composites. Additions like Si₃N₄, AlN, and ZrN have been used for hot pressing ZrB₂-based ceramics in order to inhibit grain growth at high sintering temperatures.^{10–12} Also, using WC, MoSi₂, B₄C, and C as sintering aids, pressureless sintering has become a powerful method for creating dense components.^{13–16}

As an alternative route, reactive hot pressing (RHP) has shown very good potential for low-temperature sintering.¹⁷ TiC–TiB₂ composites can be fabricated by transient plastic phase processing through RHP.¹⁸ ZrB₂–SiC composites and

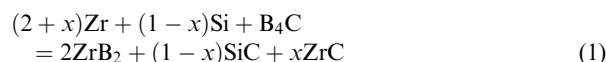
ZrB₂–SiC–ZrC composites have been successfully sintered using Zr, Si, and B₄C as starting powders.^{19,20} ZrB₂–SiC ceramics with relative densities > 95% were produced by RHP at a temperature of 1650°C using attrition-milled Zr, B, and SiC as starting powders.²¹ RHP will keep on becoming an important method in sintering UHTCs.

The addition of ZrC to ZrB₂–SiC to form a ternary composite of ZrB₂–SiC–ZrC can tailor the microstructure and properties of ZrB₂–SiC, especially the superior resistance to ablation at a high temperature.²² In the current work, ZrB₂–SiC–ZrC composites were prepared by RHP at temperatures as low as 1600°C. In this paper, the reaction sequence, the manufacturing process at low temperature, the microstructural evolution, and the mechanical properties of the low-temperature-sintered composites are investigated.

II. Experimental Procedure

(1) Powder Processing

ZrB₂–SiC–ZrC composites were prepared by RHP according to the following reaction:



The calculated volumetric compositions and the theoretical densities of the composites are listed in Table I. The theoretical density is calculated according to the rule of mixtures based on the densities of 6.09, 3.21, and 6.44 g/cm³ for ZrB₂, SiC, and ZrC, respectively. The starting powders were Zr, Si, and B₄C; their characteristics, as provided by the suppliers, are listed in Table II. The correspondent stoichiometric precursors of Zr, Si, and B₄C were weighed according to the value of *X* in Table I. Two methods were used to mix the precursor powders, and the resulting mixtures were labeled as PA and PB. For PA, the starting powders were ball milled in acetone for 24 h using ZrO₂ milling media in a plastic bottle. For PB, in order to decrease the particle size, precursor powders were planetary ball milled in acetone at 550 rpm for 8 h in a polyethylene jar, using ZrO₂ media. The powders were then dried in a rotary evaporator and sieved through a –200-mesh screen to reduce powder segregation and agglomeration. Meanwhile, pure Zr and Si were processed in the same way as PB to study the effect of milling on particle size and particle morphology.

(2) Reaction Study and Sintering

The milled powders were placed in a graphite die (30 mm × 37 mm) with a BN coating, and then uniaxially hot pressed under a vacuum atmosphere. All of the sintering studies were conducted using a graphite crucible in a resistance-heated graphite element furnace (ZT-60-22Y, Chen Hua Electric Furnace Co. Ltd., Shanghai, China). The temperature was monitored by a pyrometer focused on the graphite die. In order to study the reaction sequence during sintering, powder PA was hot pressed at 650°,

D. Butt—contributing editor

Manuscript No. 24241. Received January 20, 2008; approved April 21, 2008.

Financial support from the Chinese Academy of Sciences under the Program for Recruiting Outstanding Overseas Chinese (Hundred Talents Program), the National Natural Science Foundation of China (No. 50632070 and No. 50602048), the State Key Laboratory of High Performance Ceramics, and Superfine Microstructures of Shanghai Institute of Ceramics is gratefully acknowledged.

*Member, American Ceramic Society.

†Author to whom correspondence should be addressed. e-mail: gjzhang@mail.sic.ac.cn

Table I. Calculated Volumetric Compositions and the Expected Densities of the Composites

Reaction	Calculated composition (vol%)	Theoretical density (g/cm ³)
(2+x) Zr+(1-x)Si+B ₄ C = 2 ZrB ₂ +(1-x)SiC+x ZrC, x = 0.15628	ZrB ₂ : 73.96 SiC: 21.04 ZrC: 5	5.50

800°, 1000°, 1200°, and 1450°C at a heating rate of 10°C/min and a hold time of 1 h.

In order to obtain dense samples, both powders A and B were used. As summarized in Table III, the processing conditions varied, but generally consisted of three stages:

(1) Stage 1: The powders were heated at 10°C/min to about 900°C and held at that temperature for 1 h.

(2) Stage 2: The temperature was increased at 10°C/min to 1450°C and held for various times. A pressure of 10 MPa was applied on the samples as soon as the temperature reached 1450°C; after a half of the holding time, the pressure was increased to 20 MPa.

(3) Stage 3: The temperature was increased at 10°C/min to the final temperature of 1600°C and held for various times. The applied pressure was increased to 30 MPa at the beginning of the holding time.

Changes in the vacuum level of the furnace and shrinkage of the powder compacts were monitored and recorded during heating and hot pressing.

Table II. Characteristics of the Starting Powders

Power	Purity	Manufacturer	Particle size (m)
Zr	>98%	Beijing Mountain Technical Development Center for Non-ferrous Metals, Beijing, China	<28
Si	>99%	Yinfeng Silicon Co. Ltd., Jinan, China	<50
B ₄ C	99%	Jingangzuan Boron Carbide Co. Ltd., Mudanjiang, China	1.5

Table III. Density Developments of the Intermediate Products

	Processing conditions						Density	Relative density
	Stage 1		Stage 2		Stage 3			
	Temperature (°C)	Time (h)	Temperature (°C)	Time (h)	Temperature (°C)	Time (h)		
I (with SHS reaction)								
PB1			1450	1			3.24	59
PB2			1450	3			4.42	80.4
PB3					1600	3	4.94	89.9
PB4			1450	3	1600	1	4.86	88.4
PB5			1450	1	1600	3	5.13	93.2
PB6			1450	3	1600	3	5.34	97.3/0.6
II (without SHS reaction)								
PA1			1450	3			4.03	73.3
PA2			1450	3	1600	3	4.55	82.8
PB7	900	1	1450	1			3.38	61.5
PB8	900	1	1450	3	1600	3	4.94	89.9
PB9	900	1						

(3) Characterization

After hot pressing, the bulk density of the hot-pressed sample was determined using the Archimedes technique with water as the immersing medium. The reaction products were first pulverized in a stainless-steel die under high pressure, and then ground to fine powders in an agate mortar. The phase compositions of the powders were determined by X-ray diffractometry (XRD) using a Guinier-Hägg camera (XDC1000, Guinier-Hägg, Stockholm, Sweden) with CuK α 1 ($\lambda = 1.5405981$ Å) radiation. The sample fracture surfaces and the powders were observed by a scanning electron microscope (SEM, Hitachi S-570, Tokyo, Japan), and the polished surfaces of the samples were analyzed by an electron probe micro-analyzer (JXA-8100F, Tokyo, Japan). Powders that were scraped off the samples were studied by a transmission electron microscope (TEM; JEOL, Tokyo, Japan; JEM-2010/200CX/2100F). For the oxygen content measurement, in order to reduce the effect of the impurities, fresh chip samples were pulverized from the reaction products; powders were dried in a rotary evaporator to remove the solvent. The oxygen content of the chip samples and powders was determined by a Nitrogen/Oxygen Determinator (TC600, Leco Corporation, St. Joseph, MI). Four-point bending strength was measured on chamfered bars with a dimension of 2 mm \times 1.5 mm \times 25 mm, using inner and outer spans of 10 and 20 mm, respectively, and a crosshead speed of 0.2 mm/min. Hardness and fracture toughness of the samples were determined using Vickers indentation at a load of 10 kg and a dwell time of 10 s. Five specimens were tested for each data point. The fracture toughness was calculated using the following equation:

$$K_{IC} = P \left(\pi \left(\frac{C_1 + C_2}{4} \right) \right)^{-3/2} (tg\beta)^{-1} \quad (2)$$

where P is the load (100 N), C_1 and C_2 are the measured diagonal crack lengths (m), and β is an angle constant (68°).

III. Results and Discussion

(1) Powder Characterization

The planetary ball milling with a high rotating speed of 550 rpm not only mixes the powders efficiently but also reduces the particle size by the effect of friction and high-energy collision; the extent of this effect is closely related to the milling time. An 8-h milling caused a significant reduction in the particle size. In comparison, a 24-h ball milling just demonstrates the effect of

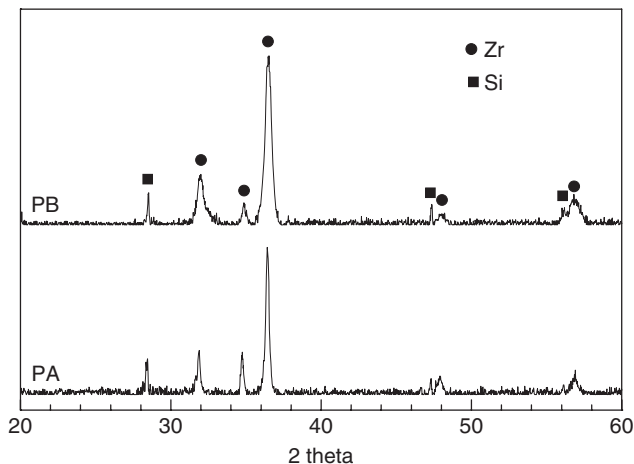


Fig. 1. X-ray diffraction patterns of the precursor powders of PA and PB.

more intimate mixing without further particle size reduction. Figure 1 shows the XRD patterns of the precursor powders PA and PB that were ball milled and planetary milled, respectively. In both XRD patterns, only two phases (Zr and Si) were detected, and no third phase is presented, implying that no appreciable reaction took place during the milling and drying process. Because of the low content and a limited scattering factor of B_4C , its peaks are not apparent. From the XRD patterns, it can be seen that the width of the Zr peaks of PB is noticeably larger than that of PA, while the width of the Si peaks showed no difference.

Two sources of peak broadening need to be considered: strain and reduced crystallite size. From the SEM images (shown in Fig. 2) of pure Zr and Si powders before and after 8-h planetary milling, it can be seen that the particle size of both Si and Zr

decreased. The particles before milling are as large as $50\ \mu\text{m}$ and have clear edges. For Si, its brittle nature makes it very easy to break into small particles (average $1\ \mu\text{m}$) with sharp edges. In contrast, Zr possesses the metals' ductile nature, and is thus relatively difficult to fracture; all of the particles, after being milled for 8 h, are plate like, with the average particle size ($5\ \mu\text{m}$) being larger than that of Si. In addition, the particles' edges are irregular. These morphology characteristics of Zr imply that there is large strain as well as a high concentration of defects in the grains, which indicates a very high reactivity. In fact, if the milling time was to be extended to 24 h, the Zr platelets could be fractured into smaller particles, but the high reactivity of Zr would make it easy to be self-ignited in air.

(2) Sintering

Figure 3 shows the vacuum level in the furnace chamber and the punch displacement during hot pressing. Although the pump was kept on during the heating process to ensure that all of the samples were heated under vacuum, reactions that involved the oxygen impurities (B_2O_3 impurities that cover the B_4C powders particles, and ZrO_2 imported during milling) took place, and gaseous phases like SiO and CO, as well as B_2O_3 , were released, which in turn increased the gas pressure and briefly eliminated the vacuum. As shown in Fig. 3(a), during the first heating stage of PA, when the temperature is below 450°C , the decrease in vacuum pressure is attributed to the degassing and dehydration of the powders. As the temperature increased, B_2O_3 , with its low melting point of 450°C , vaporized. During the short period from roughly 800° to 1200°C , there was no obvious change of vacuum, indicating that a rate balance was reached between gas released and gas pumped out. After that period, the vacuum decreased again and reached its peak value at the target temperature of 1450°C , meaning more gas phases were released from the sample.

As for PB, it can be seen from Fig. 3(b) that there are three main peaks in the vacuum curve during the heating process. The

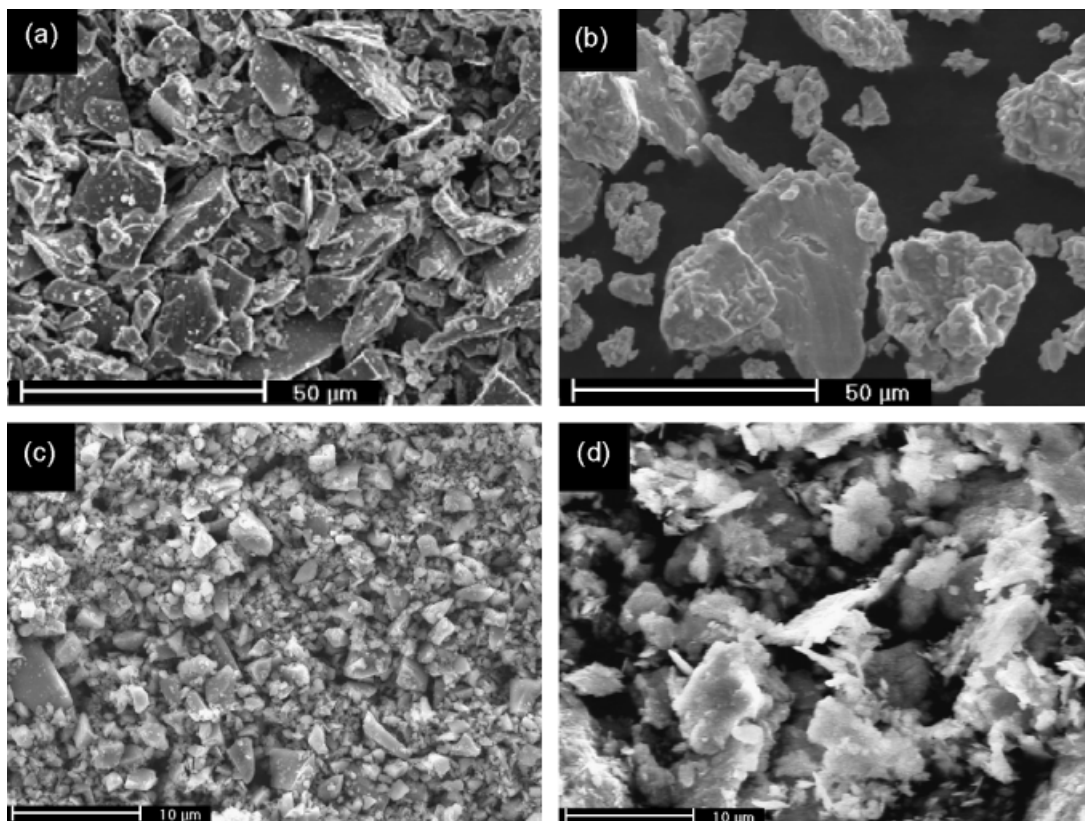


Fig. 2. Morphologies of Zr and Si powders : (a) Si powder before planetary milling; (b) Zr powder before planetary milling; (c) Si powder after planetary milling; and (d) Zr powder after planetary milling.

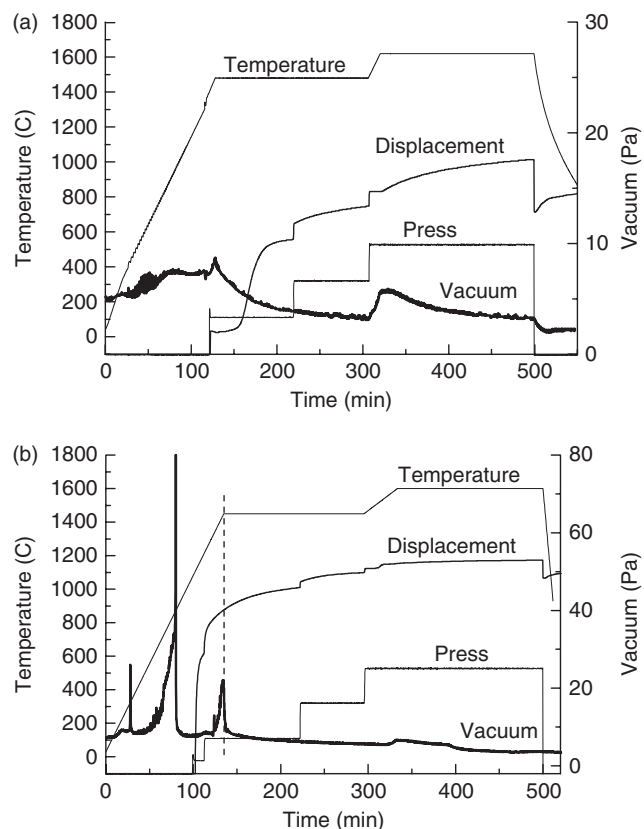


Fig. 3. Vacuum level in the furnace chamber and displacement of the punch during hot pressing.

first peak, at about 350°C, can be related to the degassing and dehydration of the fine powder after the long milling time. The second peak emerged at a temperature of roughly 900°C, and although this temperature varied each time, it always fell in the temperature range of 900°–950°C. This peak is the strongest of the three (vacuum decrease in the case of PB is more than 80 Pa), and is much more intensive than the vacuum decreases of the PA (the biggest decrease in the case of PA was no more than 5 Pa). This indicates that a possible abrupt reaction has occurred in PB. The third is similar to the peak appearing in Fig. 3(a) between 1200° and 1450°C.

As can be seen from both Figs. 3(a) and (b), the punch displacement is very sensitive to the pressure applied; each time with an increase of pressure, the displacement increased immediately. However, there is a difference in the two cases. For the former, the displacement keeps growing until the last minute of the soaking time at 1600°C. It means that the samples did not reach full density and still have a tendency to keep on shrinking. As for the latter, after a sharp increase during the initial application of pressure, the displacement increased slowly in the remaining time, and stopped growing during soaking at 1600°C. This implies that the samples have been fully densified. This observation is considered to be helpful in establishing the sintering schedule, and shows that the ZrB₂–SiC–ZrC composite can be synthesized at temperatures as low as 1600°C.

The differences in vacuum change and sample displacement during the sintering process between PA and PB reveal that different reactions occurred in the same sintering schedule. The most important difference is considered to be that which occurred at around 900°C. As a comparison, PB was heated at the same heating rate of 10°C/min, but in order to inhibit the abrupt reaction, the sample was held for 1 h at 900°C, just below the temperature at which the strongest drop in vacuum pressure appeared. It was verified that the sintering behavior of PB held at 900°C for 1 h is the same as that shown in Fig. 3(a).

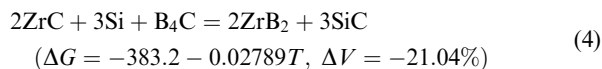
Table III shows the density values of the ZrB₂–SiC–ZrC composites sintered using different starting particles and heat-

ing schedules. All of the samples can be divided into two groups: (I) using PB as the starting powder, whose sintering behavior is consistent with that shown in Fig. 3(b); and (II) using PA or holding PB at 900°C for 1 h to inhibit the abrupt reaction that otherwise takes place, whose sintering behavior is the same as that shown in Fig. 3(a). It is interesting that only group (I) could attain superior relative density by sintering at the temperature of 1600°C (sample PB6, relative density of 97.3%), whereas the relative densities of the group (II) samples, sintered at the same temperature, remained below 90%. This result is consistent with the phenomenon observed in the samples' displacement evolution.

(3) Ignition of Self-Propagating High-Temperature Synthesis (SHS) Reaction

Figure 4 shows the XRD patterns of the intermediate products of the ZrB₂–ZrC–SiC composite heat treated at different temperatures (from 650° to 1450°C) for 1 h with a heating rate of 10°C/min in vacuum using PA as the precursor. It can be found that compared with the precursor powder before processing, there is no apparent change in the XRD pattern of PA after being heated at 650°C for 1 h. At 800°C, both ZrC and ZrB₂ had formed, with the peaks of ZrC being much higher than those of ZrB₂. Although considerable Zr and Si were still present at this temperature, by 1000°C no residual Zr could be observed, and the amount of Si was greatly reduced.

As the temperature was increased from 1000° to 1450°C, the content of ZrB₂ continued to increase while the content of ZrC decreased. The peaks of Si disappeared at 1200°C, and the peaks of SiC were detected in the XRD pattern until the temperature reached 1450°C. This result is consistent with the previous conclusion that the reaction takes place in two steps as reactions (3) and (4):²⁰



Both reactions (3) and (4) are thermodynamically favorable and highly exothermic with a negative volume change (ΔV), which indicates the tendency toward shrinkage of the specimen's dimension. Reaction (3) takes place more readily than reaction (4) because it has a larger negative value of Gibbs free energy, as seen in the fact that reaction (3) occurred at about 800°C, while reaction (4) took place at around 1200°C.

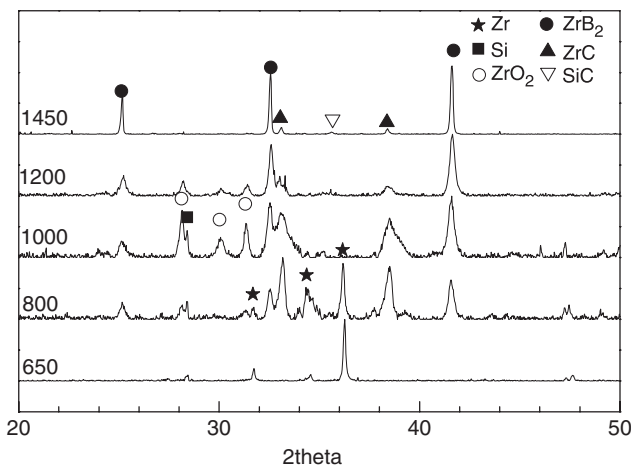
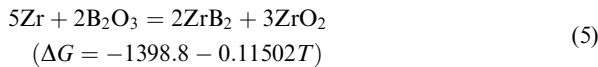


Fig. 4. X-ray diffraction patterns of the intermediate products of the ZrB₂–ZrC–SiC composite.

It should be pointed out that ZrO_2 appeared in the XRD pattern after heating to 800° , 1000° , and $1200^\circ C$. The presence of ZrO_2 can be attributed to the oxidation of the newly formed ZrC and ZrB_2 when the samples were exposed to air for the XRD test. In addition, as shown in reaction (5), Zr would first react with the B_2O_3 impurities that covered the B_4C powders particles to form ZrO_2 before reaction (2) occurs. Which factor is more important is still under research.



Reactions (1), (3), and (4) among Zr, Si, and B_4C are highly exothermic and satisfy the thermodynamic conditions for SHS processes ($T_{ad} \geq 1800$ K and $\Delta H_{298}^\circ/C_{p298} > 2000$ K)²³; hence, ZrB_2 -SiC-ZrC composites could be directly synthesized by igniting the SHS reaction. The huge change in vacuum pressure as shown in Fig. 3(b) was an indication of this ignition. Because the reaction is very exothermic, the true temperature of the sample could be very high. As a result, a great deal of B_2O_3 vaporized instantly, leading to the sharp decrease in vacuum. Figure 5(a) shows the typical example of XRD patterns of the samples that cooled down immediately after that change occurred. The peak temperature falls in the range of 900° - $950^\circ C$ as mentioned above. Only three phases were detected in the analysis of XRD patterns: ZrB_2 , SiC, and ZrC, corresponding to reaction (1). This means that the SHS reaction was ignited and completed in a rather short amount of time. Figure 5(b) shows the XRD pattern of PB that has held at $900^\circ C$ for 1 h. It coincides with PA held at 800° and $1000^\circ C$, but exhibits smaller peak widths, indicating a diffusion-controlled reaction, as a finer powder leads to a faster reaction rate and a more crystallized product. These results show that, with a heating rate of $10^\circ C/min$, PA could hardly be ignited. In contrast, the SHS ignition of PB is possible due to its fine particle size and high reactivity as mentioned above. However, by soaking at temperatures before the SHS reaction occurs, the ignition of the SHS reaction can be inhibited.

The sample (PB9) that has soaked at $900^\circ C$ for 1 h is porous and of very low strength, and powder can be scraped off easily from the sample. The powder's morphology is shown in Fig. 6(a). It is mainly large foam-like agglomerated particles (average particle size $\sim 10 \mu m$), each consisting of many smaller particles that are about $1 \mu m$. Besides these large agglomerates, particles of retained Si can also be easily found. Figure 6(b) shows the morphology of the powders that were scraped off the specimens after the SHS reaction had taken place. It is very loose, with a flocculent morphology. TEM inspection (see Fig. 7) showed that the powders are mainly aggregates of rather

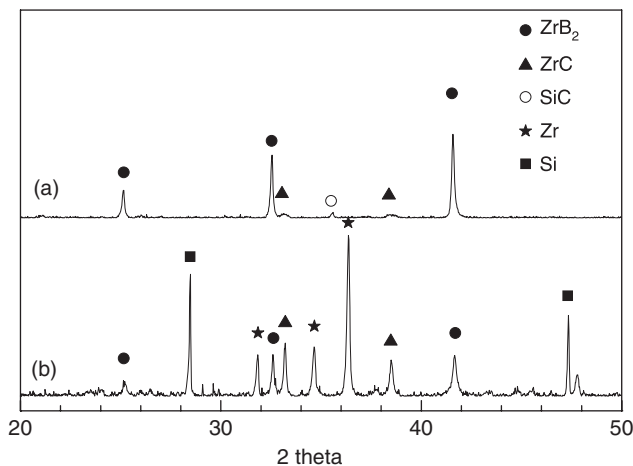


Fig. 5. X-ray diffraction patterns of samples: (a) PB after SHS reaction and (b) PB soaked at $900^\circ C$ for 1 h.

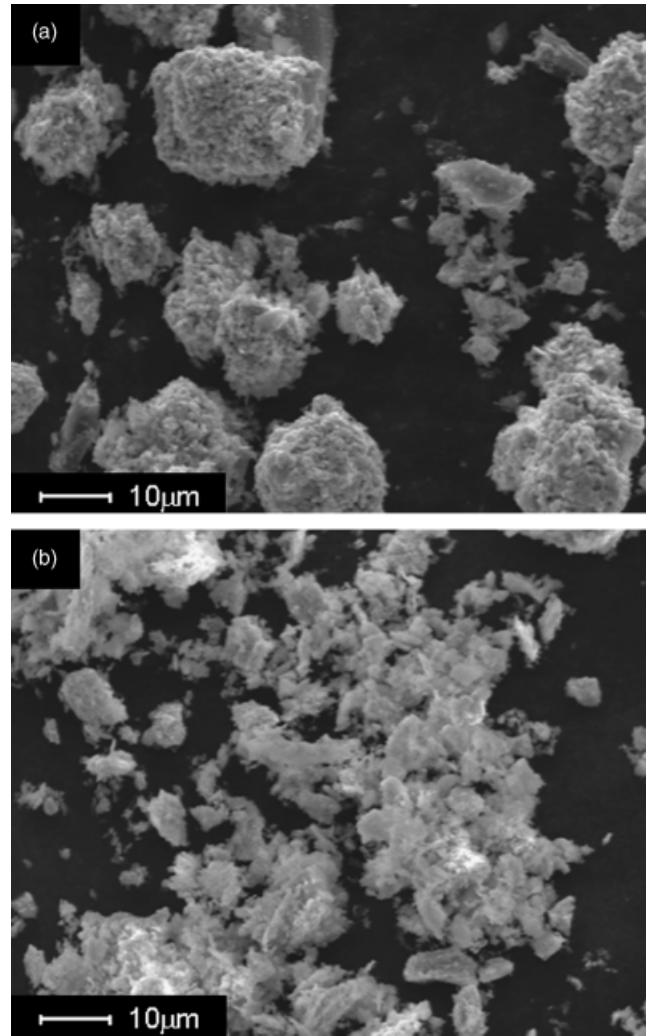


Fig. 6. Scanning electron microscopic images of powders scraped off the intermediate samples: (a) PB soaked at $900^\circ C$ for 1 h and (b) PB after ignition of SHS reaction.

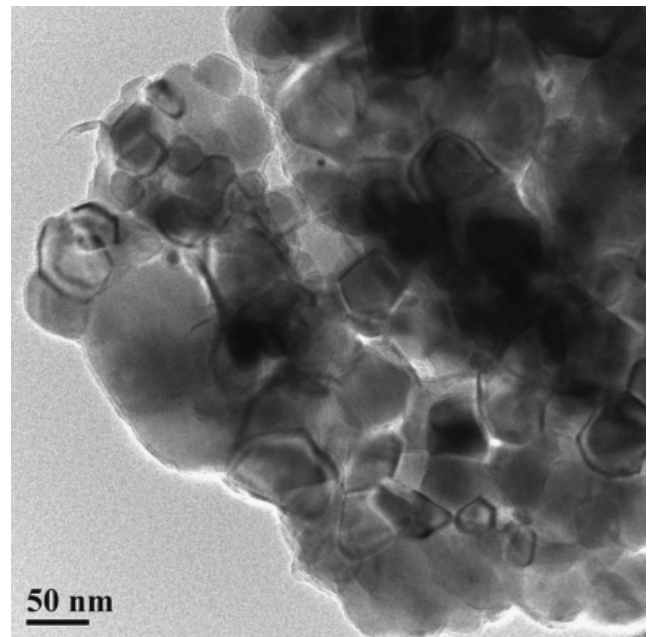


Fig. 7. Transmission electron microscopic image of PB after ignition of the SHS reaction.

fine primary particles; the average primary particle size is about 50 nm, which indicates a very high sinter-reactivity.

(4) Removal of Oxide Impurities and Densification

There are two factors that would influence the sintering behavior of this ZrB_2 -based compact. First, as discussed above, the compact underwent a diffusion-controlled reaction so that the product retains the original morphology of the starting particles. For group (II), after continuous soaking for 1 h at 1450°C , the microstructure of sample PB7 retained the characteristics of the powders obtained that soaked at 900°C for 1 h as shown in Fig. 8(a). As a result, the microstructure is still inhomogeneous with large particles in some places and small particles in others, after sintering at a higher temperature of 1600°C for 3 h, as shown in Fig. 9(a). For group (I), the homogeneity of the powder has been improved and powder with a grain size distribution in the nanoscale was obtained after the SHS reaction. Figure 8(b) shows the fine microstructure of PB1 after heating to a higher temperature of 1450°C . Composites with a homogeneous microstructure and without particle overcoarsening were obtained after sintering at a higher temperature of 1600°C for 3 h, as Fig. 9(b) shows.

Second, studies have shown that oxide impurities covering the particles would inhibit the mass diffusion and promote rapid grain coarsening. This can lead to the formation of porosity and, therefore, limit the final densities²⁴; hence, an efficient removal of oxide impurities is important to obtain fully dense composites. Combined with the observation that the decrease of vacuum in Fig. 3(a) is slower and more moderate than that of Fig. 3(b), we can conclude that the removal of oxide impurities is more efficient during the SHS reaction of group (I) than group (II) samples. Hence, the as-obtained powders in group (I) should have more cleaner surfaces, and their reactivity and mass trans-

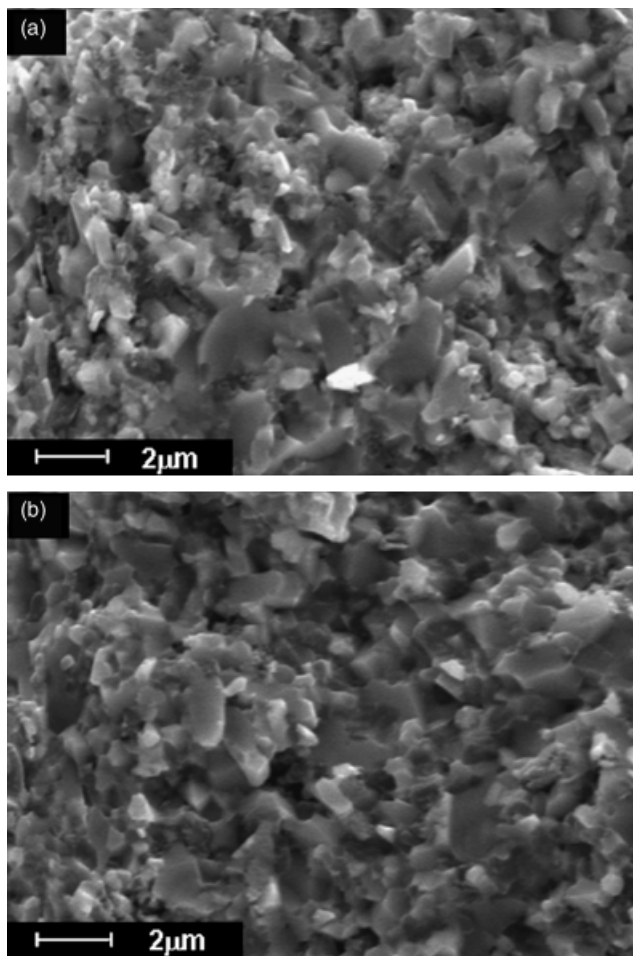


Fig. 9. Fracture morphology of samples sintered at 1600°C for 3 h: (a) PB8 and (b) PB6.

port speed during sintering are higher. In fact, only group (I) could attain a relatively fully dense (relative density of 97.3%) compact by sintering at the temperature of 1600°C . From Fig. 10(a), it can be seen that the microstructure is fine and the particle size of ZrB_2 and ZrC is $<2\ \mu\text{m}$. However, samples of group (II) that were sintered without the SHS reaction could not be densified (relative density of 89.9%). When the sintering temperature was increased to 1800°C , where the mass diffusion is enhanced by the higher temperature, a rather high relative density ($\sim 99\%$) was achieved, but the particle size became relatively large with many elongated particles (see Fig. 10(b)).

Analysis of oxygen content confirmed the above conclusion. The oxygen contents of precursor powders and the as-sintered samples are listed in Table IV. The oxygen content of PA is much lower than of PB, 0.98% and 4.46%, respectively. Because PB has a higher extent of milling, more oxidation took place during the milling. Meanwhile, the use of ZrO_2 as milling media in planetary milling yielded another source of the oxygen impurity. The oxygen content caused by ZrO_2 contamination is 1.01%, according to the weight loss of the milling media. Compared with the low value (0.94%) of PB6 that is sintered at 1600°C with occurrence of SHS, the sample densified at 1800°C without the SHS reaction has a much higher value (2.34%) of oxygen content. Also, the oxygen content of the sample that cooled down immediately after the SHS reaction decreased sharply to 1.40%. All these proved that the SHS reaction depleted the oxygen impurities efficiently.

As shown in Figs. 3(a) and (b), for both cases, after the critical temperature of about 900°C was reached during heating, the vacuum decreased, and then decreased again during the holding time. Thermodynamic calculations for reactions (6), (7), (8), and (9) showed that the retained ZrO_2 and newly formed ZrC can

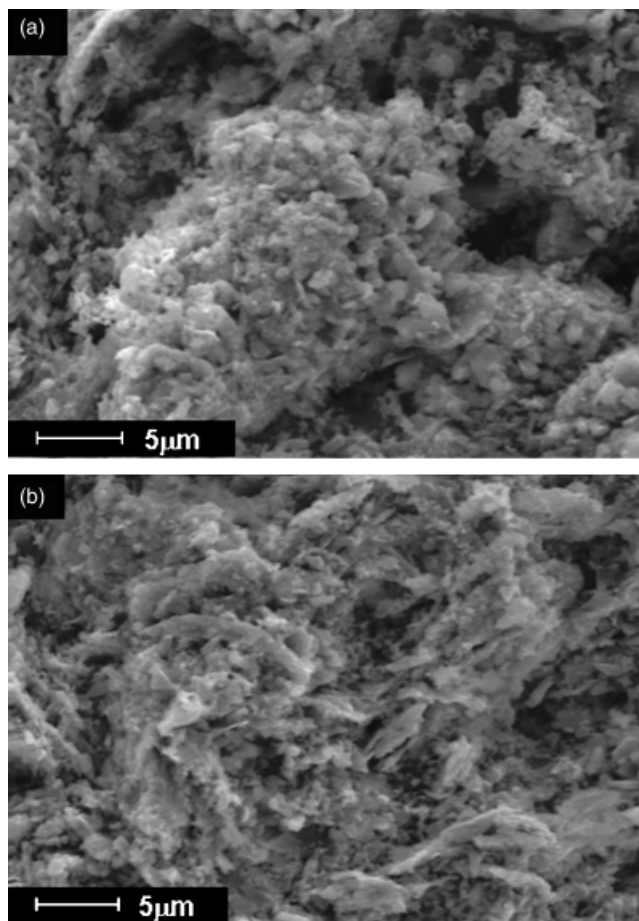


Fig. 8. Fracture morphology of samples sintered at 1450°C for 1 h: (a) PB7 and (b) PB1.

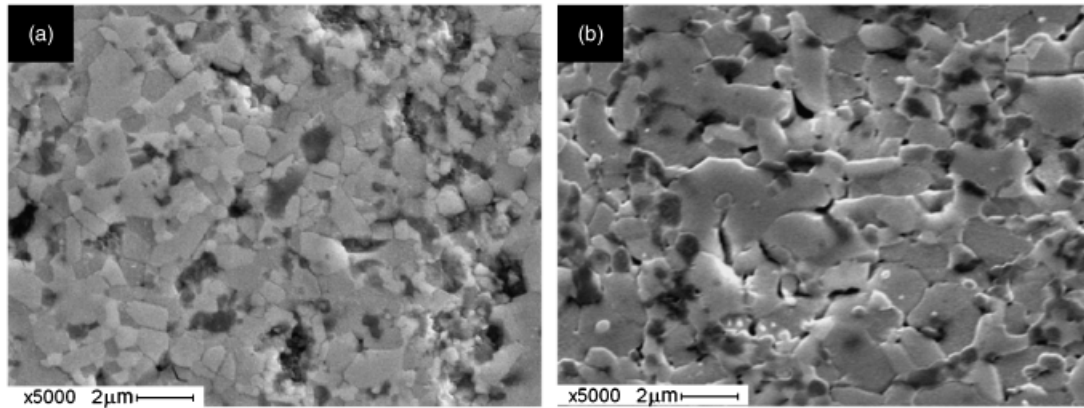
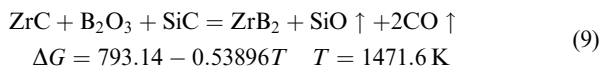
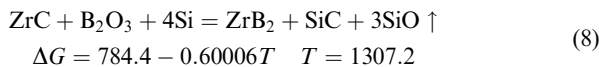
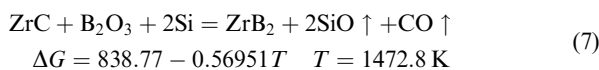
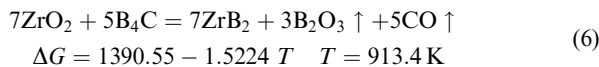


Fig. 10. Scanning electron microscopic images of the polished surface of samples after acid corrosion: (a) PB sintered at 1600°C for 3 h and (b) PB sintered at 1800°C/1 h without the SHS reaction.

Table IV. Oxygen Contents of Precursor Powders and the As-Sintered Samples

Powder	Oxygen content of PA (%)	Oxygen content of PB (%)
Powder	0.98	4.46 (imported by planetary milling)
SHS (~900°C)		1.40
PB6 (1450°C/3 h, 1600°C/3 h)		0.94
1800°C/1 h (without SHS)	0.98	2.34

also react with the remaining B₂O₃ and the unreacted B₄C and Si to form gaseous SiO and CO. These reactions are favorable at temperatures, above 900°C. As a result, during soaking at 1450° and 1600°C, the removal of oxide impurities was enhanced, and the driving force for the densification increased at the same time.



(5) Mechanical Properties

The mechanical properties of the composite (PB6) are listed in Table V. The hardness is comparable to that of the conventional hot-pressed samples. The fracture toughness is high compared with the other ZrB₂-SiC-based composites sintered by RHP.^{21,25}

Table V. Mechanical Properties of ZrB₂-SiC-ZrC Densified at 1600°C

	ZrB ₂ -SiC-ZrC
Density (%)	97.3
Open porosity (%)	0.6
Hardness (GPa)	17.2 ± 0.8
Fracture toughness (MPa · m ^{1/2})	5.2 ± 0.4
Flexural strength (MPa)	747 ± 101

The flexural strength, although lower than conventional hot-pressed samples,⁹ is higher than the other high-temperature reactive-sintered composites^{21,25}; this can be attributed to the fine microstructure as shown in Fig. 10(a).

IV. Conclusions

A fully dense ZrB₂-SiC-ZrC ceramic was produced by RHP at temperatures as low as 1600°C, the lowest sintering temperature reported thus far. The relative density is 97.3% with an open porosity of 0.6%. The enhanced densification by low-temperature RHP was attributed to three main reasons:

(1) The planetary ball milling with a high rotation speed of 550 rpm can not only mix the powders efficiently, but can also reduce the particle size by the effect of friction and high-energy collisions, as the resulting mixture is fine and has a very high reactivity.

(2) With a heating rate of 10°C/min, the SHS reaction will be ignited instead of reacting in two steps. The as-obtained fine powders with fresh surfaces have high reactivity, and thus provide a high driving force in densification.

(3) Studies on samples' sintering behavior have shown that the removal of oxide impurities is critical to reducing the densification temperature. The removal of oxide impurities is especially efficient during the SHS reaction, promoting the mass transport during the heating process without significant particle coarsening.

Vickers hardness for the fully dense RHP materials was 17.2 GPa, which is lower than conventionally hot-pressed articles and was due to the porosity of the sample. The fracture toughness of the RHP materials was 5.2 MPa · m^{1/2}. This high value is attributed to the low level of oxide impurities. The flexure strength was 747 MPa, a relatively high value considering its low sintering temperature, resulting from the reduced particle size and lower amount of grain boundary phases.

Acknowledgments

We are grateful to Alex Spring for his careful corrections of this manuscript.

References

- 1T. A. Jackson, D. R. Eklund, and A. J. Fink, "High Speed Propulsion: Performance Advantage of Advanced Materials," *J. Mater. Sci.*, **39**, 5905-13 (2004).
- 2D. M. Van Wie, D. G. Drewry Jr., D. E. King, and C. M. Hudson, "The Hypersonic Environment: Required Operating Conditions and Design Challenges," *J. Mater. Sci.*, **39**, 5915-24 (2004).
- 3R. Savino, M. De S. Fumo, D. Paterna, and M. Serpico, "Aerothermodynamic Study of UHTC-Based Thermal Protection Systems," *Aerosp. Sci. Technol.*, **9**, 151-60 (2005).
- 4K. Upadhyay, J.-M. Yang, and W. P. Hoffman, "Materials for Ultrahigh Temperature Structural Applications," *Am. Ceram. Soc. Bull.*, **76** [12] 51-6 (1997).
- 5E. Wuchina, M. Opeka, S. Causey, K. Buesking, J. Spain, A. Cull, J. Routbort, and F. Guitierrez-Mora, "Designing for Ultrahigh-Temperature Applications:

The Mechanical and Thermal Properties of HfB_2 , HfC_x , HfN_x and $\alpha\text{Hf(N)}$," *J. Mater. Sci.*, **39**, 5939–49 (2004).

⁶A. K. Kuriakose and J. L. Margrave, "The Oxidation Kinetics of Zirconium Diboride and Zirconium Carbide at High Temperatures," *J. Electrochem. Soc.*, **117**, 827–31 (1964).

⁷W. G. Fahrenholtz and G. E. Hilmas, "Refractory Diborides of Zirconium and Hafnium," *J. Am. Ceram. Soc.*, **90** [5] 1347–64 (2007).

⁸W. C. Tripp, H. H. Davis, and H. C. Graham, "Effect of a SiC Addition on the Oxidation of ZrB_2 ," *Am. Ceram. Soc. Bull.*, **52** [8] 612–6 (1973).

⁹A. L. Chamberlain, W. G. Fahrenholtz, G. E. Hilmas, and D. T. Ellerby, "High-Strength Zirconium Diboride-Based Ceramics," *J. Am. Ceram. Soc.*, **87** [6] 1170–2 (2004).

¹⁰F. Monteverde and A. Bellosi, "Effect of the Addition of Silicon Nitride on Sintering Behaviour and Microstructure of Zirconium Diboride," *Scr. Mater.*, **46**, 223–8 (2002).

¹¹F. Monteverde and A. Bellosi, "Beneficial Effects of AlN as Sintering Aid on Microstructure and Mechanical Properties of Hot-pressed ZrB_2 ," *Adv. Eng. Mater.*, **5** [7] 508–12 (2003).

¹²F. Monteverde and A. Bellosi, "Development and Characterization of Metal-Diboride-Based Composites Toughened with Ultra-Fine SiC Particulates," *Solid State Sci.*, **7** [5] 622–30 (2005).

¹³A. L. Chamberlain, W. G. Fahrenholtz, and G. E. Hilmas, "Pressureless Sintering of Zirconium Diboride," *J. Am. Ceram. Soc.*, **89** [2] 450–6 (2006).

¹⁴D. Sciti, F. Monteverde, S. Guicciardi, G. Pezzotti, and A. Bellosi, "Microstructure and Mechanical Properties of ZrB_2 - MoSi_2 Ceramic Composites Produced by Different Sintering Techniques," *Mater. Sci. Eng. A*, **434**, 303–9 (2006).

¹⁵S. C. Zhang, G. E. Hilmas, and W. G. Fahrenholtz, "Pressureless Densification of Zirconium Diboride with Boron Carbide Additions," *J. Am. Ceram. Soc.*, **89** [5] 1544–50 (2006).

¹⁶S. M. Zhu, W. G. Fahrenholtz, G. E. Hilmas, and S. C. Zhang, "Pressureless Sintering of Carbon-Coated Zirconium Diboride Powders," *Mater. Sci. Eng. A*, **459**, 167–71 (2007).

¹⁷G. J. Zhang, M. Ando, J. F. Yang, T. Ohji, and S. Kanzaki, "Boron Carbide and Nitride as Reactants for In Situ Synthesis of Boride-Containing Ceramic Composites," *J. Eur. Ceram. Soc.*, **24**, 171–8 (2004).

¹⁸M. W. Barsour and B. Houg, "Transient Plastic Phase Processing of Titanium-Boron-Carbon Composites," *J. Am. Ceram. Soc.*, **76** [6] 1445–51 (1993).

¹⁹G.-J. Zhang, Z.-Y. Deng, N. Kondo, J.-F. Yang, and T. Ohji, "Reactive Hot Pressing of ZrB_2 -SiC Composites," *J. Am. Ceram. Soc.*, **83** [9] 2330–2 (2000).

²⁰W.-W. Wu, G.-J. Zhang, Y.-M. Kan, and P.-L. Wang, "Reactive Hot Pressing of ZrB_2 -SiC-ZrC Ultra High-Temperature Ceramics at 1800°C," *J. Am. Ceram. Soc.*, **89** [9] 2967–9 (2006).

²¹A. L. Chamberlain, W. G. Fahrenholtz, and G. E. Hilmas, "Low-Temperature Densification of Zirconium Diboride Ceramics by Reactive Hot Pressing," *J. Am. Ceram. Soc.*, **89** [12] 3638–45 (2006).

²²B. J. White and M. J. Kauffman U.S. Patent No. 5,750,450, 1998.

²³Z. A. Munir, "Synthesis of High Temperature Materials by Self-Propagating Combustion Methods," *Am. Ceram. Soc. Bull.*, **67**, 342–9 (1988).

²⁴S. Baik and P. F. Becher, "Effect of Oxygen Contamination on Densification of TiB_2 ," *J. Am. Ceram. Soc.*, **70** [8] 527–30 (1987).

²⁵J. W. Zimmermann, G. E. Hilmas, and W. G. Fahrenholtz, "Fabrication and Properties of Reactively Hot Pressed ZrB_2 -SiC Ceramics," *J. Eur. Ceram. Soc.*, **27**, 2729–36 (2007). □